Available online at www.sciencedirect.com
SCIENCE DIRECT®
Electric Power Systems Research 75 (2005) 17–27
ELECTRIC POWER SYSTEMS RESEARCH
www.elsevier.com/locate/epsr

# Operating capability of long AC EHV transmission cables

Roberto Benato *, Antonio Paolucci [1]

*University of Padova, Department of Electrical Engineering, Via Gradenigo 6/A, 35131 Padova, Italy*

Received 29 April 2004; accepted 23 November 2004
Available online 18 April 2005

**Abstract**

The operating constraints involved in power transmission of long AC cable links are presented and here throughout developed. The possibility of transmitting high power rating is examined and the transmission length limits are evaluated. The procedure, which uses the great computation and graphical facilities of modern computers, is essentially based on the classical transmission equations and their pertaining diagrams. It has been particularly applied to XLPE cables and gas-insulated lines but it is worth applying to any distributed-parameter transmission line (including overhead lines). The capability chart proposed in the paper is a useful tool to highlight the operating characteristics of a cable link and a guide to evaluate the results of different degrees of reactive compensation. The authors hope that the results can offer the transmission system operators very effective means in order to evaluate the existing and future underground cable links.


*Keywords:* XLPE cable; EHV transmission lines; Underground technology; Gas insulated lines

## 1. Introduction

Deregulation of the electricity supply markets and growing environmental awareness stress the necessity of new transmission line solutions alternative to traditional overhead lines. So the transmission scenario is paying a great attention to the underground technologies. In particular, the use of XLPE AC cable lines seems very promising for new links [1–3]. EHV cables can be used mainly for power transmission in large urban heavily populated agglomerations, as feeders in outdoor substations, and as generator bus-ducts. The first major (i.e. where a significant number of joints is required) XLPE cable systems have been in service since 1997 at 400 kV and 2000 at 500 kV. Since those dates, the importance and the interest on these applications are increased and deserve a very careful consideration.

Another promising technology is represented by cables with gas mixture insulation (the so called gas insulated lines (GIL)): the world installations amount today roughly to 100 km and the maximum line length is 3.3 km even if much longer runs are under study [4].

Hence, in the future the variety of employed technologies in the EHV transmission could be much more than now being the network chiefly constituted by overhead lines. Thus, it results fundamental to give the transmission system operators simple but precise engineering means to evaluate the transmission operating characteristics of long AC cable links.

## 2. Settlement of the question

The main function of a cable in a EHV/HV network (as well as any transmission line) is to transmit active power $P$ with a small amount of inductive power $Q$.

Moreover, it is well known that a long service life can be reached only with these constraints in any point along the cable:

- Avoiding that the currents exceed the cable ampacity $I_c$, meant as the current carrying capacity (depending upon the installation conditions) under stated thermal conditions without degradation.

* Corresponding author. Tel.: +39 049 8277532; fax: +39 049 8277599.
*E-mail address:* roberto.benato@unipd.it (R. Benato).
[1] Tel.: +39 049 8277516; fax: +39 049 8277599.

0378-7796/$ – see front matter © 2005 Elsevier B.V. All rights reserved.
doi:10.1016/j.epsr.2004.11.011

Table 1
Data of 400 kV XLPE cables under study

| | Cable #a | Cable #b |
|---|---|---|
| Cross sectional area (mm$^2$) | 2500 Cu | 630 Cu |
| Conductor diameter (mm) | 65.0 | 30.8 |
| Conductor screen diameter (mm) | 71.6 | 32.8 |
| Insulation diameter (mm) | 122.0 | 92.8 |
| Insulation screen diameter (mm) | 128.3 | 94.8 |
| Metallic shield diameter (mm) | 130.9 Al | 101.8 Pb |
| Jacket of PE diameter (mm) | 142.5 | 117 |
| Overall diameter (mm) | 142.5 | 117 |
| Total mass (kg/m) | 37 | 28 |

- Avoiding that the phase-to-earth voltages $|\underline{U}_o|$ exceed the highest rms. Voltage $U_m/\sqrt{3}$ (Insulation Co-ordination International Standard) for cable both on-load and no-load conditions.

It is evident that foreseeing any operating conditions is rather impossible; notwithstanding, reasonable essential criteria are generally considered not to exceed, during operation, the ampacity limits at both ends (S for *Sending-end* and R for *Receiving-end*) and to assure a phase-to-earth voltage level in one of the two ends (in this paper S will be always chosen):

$$|\underline{I}_R| \leq I_c \quad (1)$$

$$|\underline{I}_S| \leq I_c \quad (2)$$

$$|\underline{U}_{oS}| = U_{oc}. \quad (3)$$

In the following investigations, where $U_m = 420$ kV, it has retained the level $U_{oc} = 230\,\text{kV} = 95\%\ U_m/\sqrt{3}$.

A throughout analysis of the cable operating characteristics with the aforementioned constraints has been presented in [5], which constitutes (chiefly by means of a general abacus) one of the first elegant (dated 1986) approaches. It has been a strong suggestion for the authors.

By a purely theoretical point of view, any cable line is an asymmetrical multiconductor system because of both the consideration of the shields and asymmetrical laying arrangements.

Nevertheless, since in the EHV cable line laying a lot of phase transpositions and cross-bondings are adopted, in this formulation a single-phase positive sequence two-port network will be simply considered.

Let's consider a uniform transmission line with distributed parameters: the starting point is a rigorous application of the famous transmission formulae (solution of the telegraphist's equations) first written in 1876 by Oliver Heaviside [6] and then used, rearranged and divulged by Steinmetz [7], Rössler [8], La Cour [9]:

$$\underline{U}_{oS} = \underline{A} \cdot \underline{U}_{oR} + \underline{B} \cdot \underline{I}_R \quad (4)$$

$$\underline{I}_S = \underline{C} \cdot \underline{U}_{oR} + \underline{A} \cdot \underline{I}_R; \quad (5)$$

(the per unit method will not be used in this paper to achieve higher engineering concreteness in terms of line operation).

Tables 1 and 2 report the main data for two different EHV #a and #b cables.

Firstly, cable #a will be considered.

## 3. First analysis: $\underline{U}_{oS}$ and $|\underline{I}_R|$ constrained

A first analysis on the possible operating conditions can be performed if both the current magnitude at R and the voltage phasor $\underline{U}_{oS}$ at S are constrained as follows:

$$\underline{I}_R = (I_c \angle 0) = (1.6\,\text{kA} \angle 0) \quad \text{on the real axis}$$

$$\underline{U}_{oS} = (U_o \angle \delta) = (230\,\text{kV} \angle \delta) \quad \delta = 0\text{–}2\pi$$

so that the remaining quantities $\underline{U}_{oR}$ and $\underline{I}_S$ can be determined (see (A3) in Appendix A) by means of subsequent equations:

$$\underline{U}_{oR} = \frac{1}{\underline{A}} \cdot \underline{U}_{oS} - \frac{\underline{B}}{\underline{A}} \cdot \underline{I}_R \rightarrow \underline{U}_{oR} = \frac{1}{\underline{A}} \cdot (230\,\text{kV} \angle \delta) - \frac{\underline{B}}{\underline{A}} \cdot (1.6\,\text{kA} \angle 0) \quad (6)$$

$$\underline{I}_S = \frac{\underline{C}}{\underline{A}} \cdot \underline{U}_{oS} + \frac{1}{\underline{A}} \cdot \underline{I}_R \rightarrow \underline{I}_S = \frac{\underline{C}}{\underline{A}} \cdot (230\,\text{kV} \angle \delta) + \frac{1}{\underline{A}} \cdot (1.6\,\text{kA} \angle 0) \quad (7)$$

Table 2
Parameters of 400 kV XLPE cables under study

| | | Cable #a | Cable #b |
|---|---|---|---|
| Cross sectional area | (mm$^2$) | 2500 Cu | 630 Cu |
| Installation | | Directly buried with spacing 0.35 m | Directly buried trefoil spacing 0.12 m |
| Per unit length resistance of phase conductor at 90 °C | $r$ (mΩ/km) | 10.8 | 36 |
| Per unit length series inductance | $\ell$ (mH/km) | 0.571 | 0.460 |
| Per unit length shunt leakance (50 Hz) with loss factor $\tan\delta = 0.0007$ | $g$ (nS/km) | 53 | 27 |
| Per unit length shunt capacitance with $\varepsilon_r = 2.3$ | $c$ (μF/km) | 0.240 | 0.123 |
| Characteristic impedance | $\underline{Z}_0$ (Ω) | $48.84\angle{-.03}$ rad | $62.01\angle{-.12}$ rad |
| Propagation factor | $\underline{k}$ (km$^{-1}$) | $(0.1 + j3.7) \times 10^{-3}$ | $(0.3 + j2.4) \times 10^{-3}$ |
| Surge impedance loading at 400 kV | SIL (MVA) | 3276 | 2577 |
| Capacitive current related to $U_o = 400\,\text{kV}/\sqrt{3}$ | $I_{cap}$ (A/km) | 17.40 | 8.92 |
| Ampacity | $I_c$ (A) | 1600 | 650 |

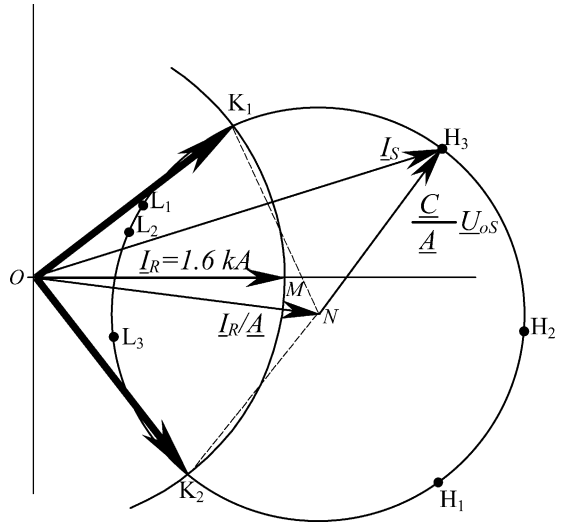


Fig. 1. Phasorial diagram of the Eq. (7) with 1.6 kA ampacity at R.

In particular, Eq. (7) gives the phasorial diagram of Fig. 1 (where only for graphical purpose, point *N* has been placed sensibly far from point *M*). The foregoing diagram shows, once fixed $\underline{I}_R = 1.6\,\text{kA}$ on the real axis, how the angle $\delta$ of $\underline{U}_{oS} = (230\,\text{kV}\angle\delta)$ can value the whole interval 0–$2\pi$ giving rise to two different groups:

(i) any regimes with $|\underline{I}_S| < 1.6\,\text{kA} = |\underline{I}_R|$ compatible with the cable ampacity (e.g. see the phasors $OL_1$, $OL_2$ and $OL_3$);
(ii) any regimes with $|\underline{I}_S| > 1.6\,\text{kA}$ not allowable (e.g. see the phasors $OH_1$, $OH_2$ and $OH_3$).

In particular, the phasors $OK_1$ and $OK_2$ which yield at $\delta_1 = 21.08^\circ$ and $\delta_2 = 158.9^\circ$, respectively (when considering cable #a with $d = 60$ km) correspond to $|\underline{I}_S| = 1.6\,\text{kA} = |\underline{I}_R|$, and concern two very meaningful regimes for power flows between S and R (see Section 6).

It is trivial that the calculation of $\underline{U}_{oR}$ by means of (6) allows individuating and consequently warning of possible operations with too high voltages (dangerous for the insulation) or too low voltages (unsuitable for operation). At the end of this first analysis, an allowable group of complex power at S and at R becomes known.

## 4. Second analysis: $\underline{U}_{oS}$ and $|\underline{I}_S|$ constrained

In order to complete the analysis of the possible operating conditions, let us consider the allowable regimes when (beyond the phasor $\underline{U}_{oS}$) the sending-end current $|\underline{I}_S|$ is fixed at the cable ampacity $I_c$. By means of (8) and (9) (see (A4) in Appendix A)

$$\underline{U}_{oR} = \underline{A}\cdot\underline{U}_{oS} - \underline{B}\cdot\underline{I}_S \rightarrow \underline{U}_{oR} = \underline{A}\cdot(230\,\text{kV}\angle\vartheta) - \underline{B}\cdot(1.6\,\text{kA}\angle 0) \quad (8)$$

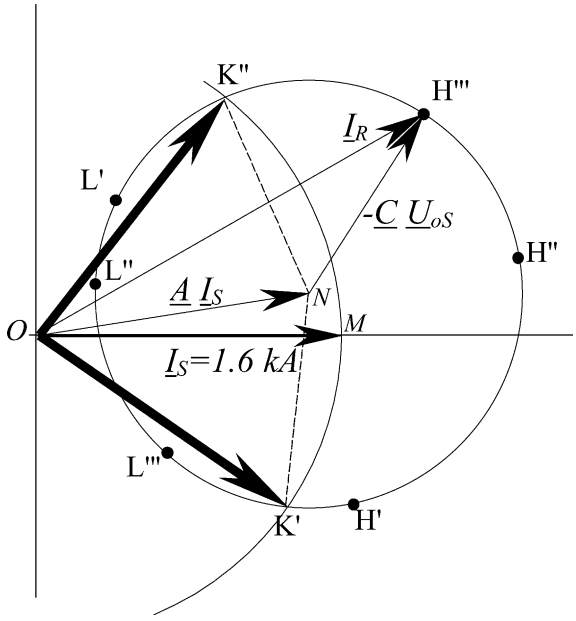


Fig. 2. Phasorial diagram of Eq. (9) with 1.6 kA ampacity at S.

$$\underline{I}_R = -\underline{C}\cdot\underline{U}_{oS} + \underline{A}\cdot\underline{I}_S \rightarrow \underline{I}_R = -\underline{C}\cdot(230\,\text{kV}\angle\vartheta) + \underline{A}\cdot(1.6\,\text{kA}\angle 0) \quad (9)$$

it is possible to analyze the effects of $|\underline{I}_S| = 1.6\,\text{kA}$ (on the real axis) and of $\underline{U}_{oS} = (230\,\text{kV}\angle\vartheta)$, where $\vartheta$ (angle of $\underline{U}_{oS}$ with respect to $\underline{I}_S$) ranging between 0 and $2\pi$. Eq. (9) can be visualized by means of the phasor diagram of Fig. 2. This diagram shows, once fixed $\underline{I}_S = 1.6\,\text{kA}$ on the real axis, how the angle $\vartheta$ of $\underline{U}_{oS} = (230\,\text{kV}\angle\vartheta)$ can value the whole interval 0–$2\pi$ giving rise to two different groups:

(iii) any regimes with $|\underline{I}_R| < 1.6\,\text{kA}$ compatible with the cable ampacity (e.g. OL′, OL″ and OL‴);
(iv) any regimes with $|\underline{I}_R| > 1.6\,\text{kA}$ not allowable (e.g. OH′, OH″ and OH‴).

In particular, the phasors OK′ and OK″ which yield at $\vartheta' = 197.1^\circ$ and $\vartheta'' = 343.1^\circ$, respectively (when considering cable #a with $d = 60$ km) individuate again two regimes (as $OK_2$ and $OK_1$ in the first analysis) with $|\underline{I}_R| = 1.6\,\text{kA} = |\underline{I}_S|$. In addition, the use of (8) allows warning of unsatisfactory voltage levels (too high or too low) at R. At the end of this second analysis, another allowable group of complex power at S and at R becomes known.

## 5. Voltages and currents along the cable

The knowledge of the currents and voltages at sending-end S and receiving-end R is not completely exhaustive of the whole electric behaviour of cable: in fact it is important to examine the currents and voltages along the cable in order to investigate possible points exceeding the fixed current and

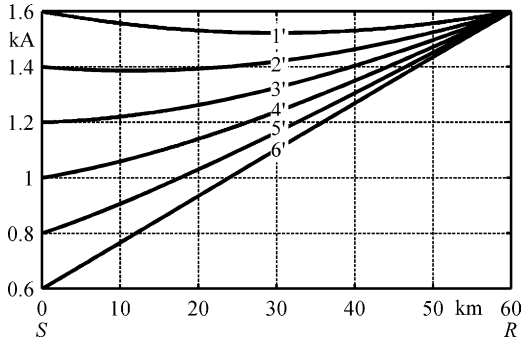


Fig. 3. Current magnitudes along the cable #a with ampacity at R (I analysis).

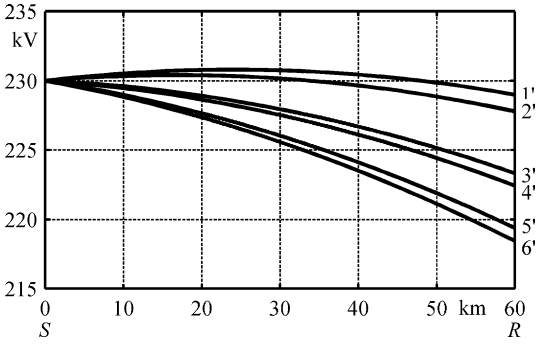


Fig. 4. Voltage magnitudes along the cable #a with ampacity at R (I analysis).

voltage limits; to this aim, the use of (A5) could be suitable. Fig. 3 shows for cable #a with $d = 60$ km the behaviour of the current along the cable in some allowable cases by the "first analysis": it is of note the curve 1′ (see point $K_1$ in Fig. 1) where both the end currents have same magnitudes equal to the ampacity. The other curves 2′–6′ regard other regimes (e.g. current phasors as OL of Fig. 1) not exceeding the ampacity along the cable. Fig. 4 shows the voltages along the cable in the same regimes; analogously, Figs. 5 and 6 show the results along the cable for some allowable regimes by the "second analysis".

These kinds of analysis along the line performed for other cables have shown analogous behaviours since the ampacity is much lower than the "natural current" $I_n = U_{oc}/|\underline{Z}_0|$. It seems that this fact has passed unobserved.

In any case, the mid-line values $\underline{U}_{oT}$ and $\underline{I}_T$ included into the matrix analysis (A8) and (A9) can give a suggestion for investigations in further points.

In order to complete the operating analyses, the current and voltage in no-load condition must be evaluated. By setting $\underline{I}_R = 0$ into (6) and (7), the no-load voltage and current can

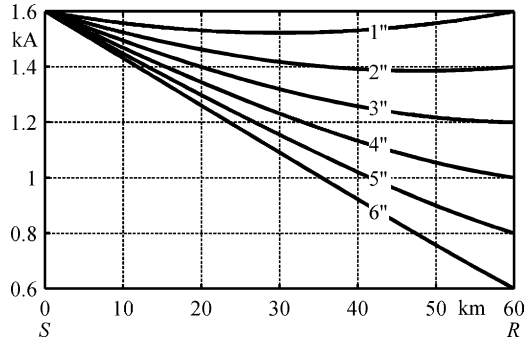


Fig. 5. Current magnitudes along the cable #a with ampacity at S (II analysis).

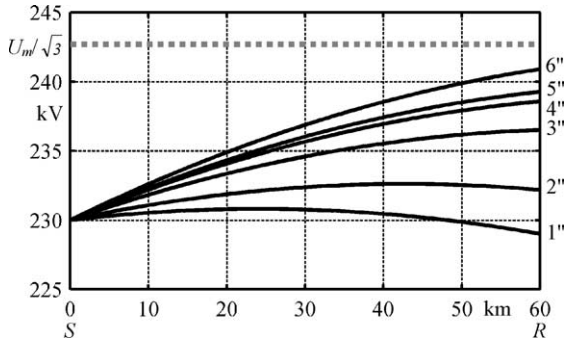


Fig. 6. Voltage magnitudes along the cable #a with ampacity at S (II analysis)

be computed as follows:

$$(\underline{U}_{oR})_{\underline{I}_R=0} = \frac{1}{\underline{A}} \cdot \underline{U}_{oS}; \qquad (\underline{I}_S)_{\underline{I}_R=0} = \frac{\underline{C}}{\underline{A}} \cdot \underline{U}_{oS}\underline{U}_{oS}. \quad (10)$$

In particular, (see, Table 3) for cable #a, the limit length for no-load voltage is $d_U = 87.75$ km and that for no-load current is $d_I = 88.95$ km.

## 6. Power capability chart

The performing of the numerical analysis in Sections 3–5 does not present any problem; particular attention must be devoted to the classification of numerous computed regimes in order to single out those technically allowable and to perform curves which are helpful for evaluating and eventually increasing the transmission power capability. In this regard, the curves in Fig. 7 can give (not withstanding their graphical simplicity) very meaningful information on cable #a power capability features varying its length (30, 60 and 90 km).

Table 3
Current and voltage magnitudes in no-load condition

| Cable #a | | Cable length $d$ (km) | | | | | |
|---|---|---|---|---|---|---|---|
| | | 30 | 60 | **87.75** | **88.95** | 90 | 120 |
| No-load at R; $\|U_{oS}\| = 230$ kV | Current magnitude at S (kA) | 0.52 | 1.06 | 1.58 | **1.60** | 1.62 | 2.23 |
| | Phase-to-earth voltage magnitude at R (kV) | 231.4 | 235.7 | **242.5** | 243.8 | 243.2 | 254.3 |

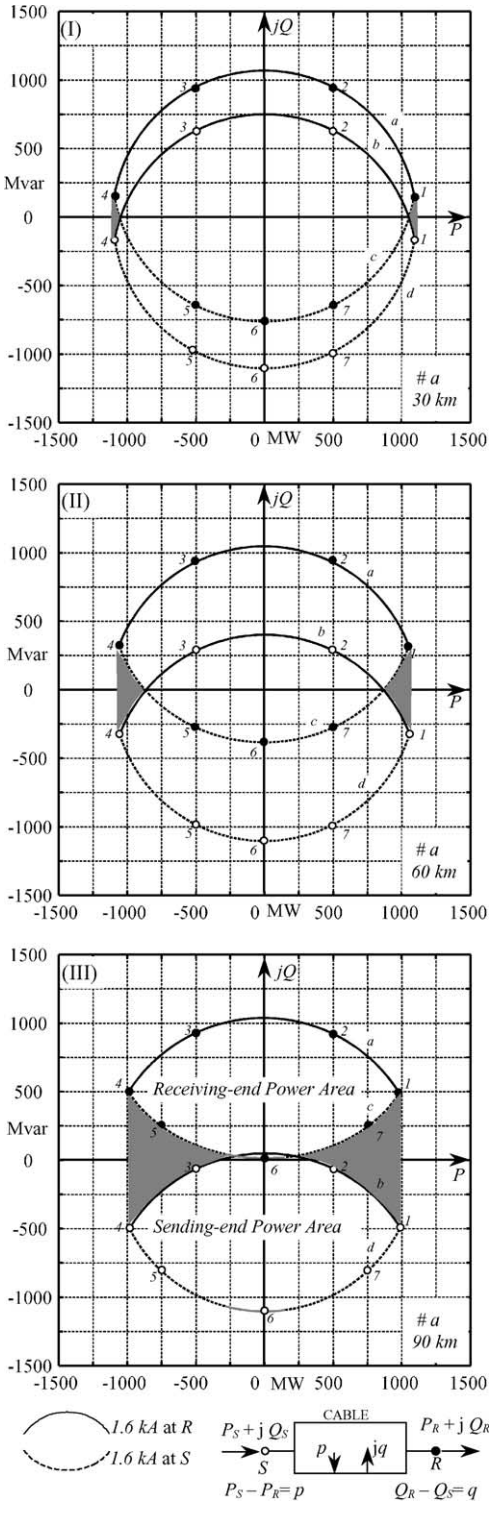


Fig. 7. Power capability charts for cable #a.

- By using the criteria of Section 3, the regimes compatible with the constraints $|\underline{I}_R| = 1.6$ kA and $|\underline{I}_S| = 1.6$ kA have been evaluated and their receiving-end complex power (e.g. points • 1–4) has been reported forming the solid lines a (see Fig. 7), whilst the corresponding sending-end complex power (e.g. points **o** 1–4) forming the solid line b.
- Analogously, by analysing the regimes $|\underline{I}_S| = 1.6$ kA and $|\underline{I}_R| \leq 1.6$ kA, according to Section 4, the dashed curves c and d have been drawn; the curve c represents the receiving-end complex power (e.g. points • 4–7, 1) and d the sending-end complex power (e.g. points **o** 4–7, 1).

Therefore, once fixed the cable ampacity at 1.6 kA, the contours a–c set the boundaries of allowable receiving-end power area whereas the contours b–d that of allowable sending-end power. As it can be gathered by power balance of Fig. 7, each sending-end power gives $P_S$ just higher than $P_R$ (since the active power losses $p$ are low) but $Q_S$ much inferior to $Q_R$ (since the cable itself generates high inductive power $q$).

In particular, points 1 and 4 (maximum active power flow between S and R) correspond to the K regimes of Figs. 1 and 2. The shadowed areas in the diagrams of Fig. 7 highlight how the power flows with high $\cos\varphi$ are more and more limited while increasing the cable length (up to almost zeroed as in Fig. 7III). This seriously jeopardizes the chief aim of the transmission link most of all in the proximity of ampacity limit. By this important point of view, the length of 25–30 km (see Fig. 7I) can be already considered as a length limit [5].

Fig. 8 shows the dramatic worsening of permissible power factor with $d = 120$ km.

However, this length would result not allowed because of no-load condition: the point O (namely $P_R + jQ_R = 0$) lays very far from the *Receiving-end Power Area*, as Table 3 confirms showing a no-load current of 2.23 kA at S and a phase-to-ground voltage of 254.3 kV at R.

On the contrary, strong reactive power flows (see Fig. 7) are possible, but they are often not convenient by an economic point of view and hence less important in the normal network operation. Exclusively in the neighbourhoods of point 6 of Fig. 7III (grey-solid lines) the regimes request too high voltages at R ($U_{oR} > U_m/\sqrt{3} = 242.5$ kV).

Fig. 7III also highlights very well the no-load current limit at S when R is not loaded: it is sufficient to note that the receiving-end power $P_R + jQ_R = 0$ lays (point • 6) almost on

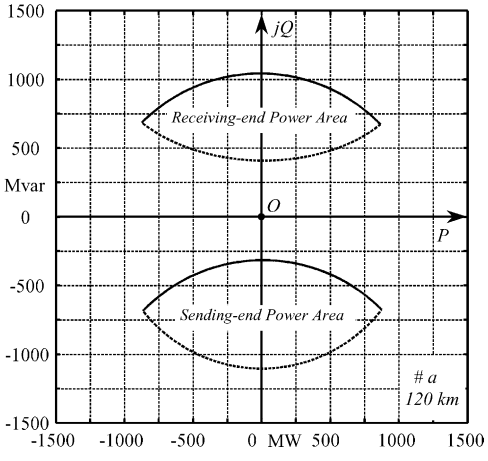


Fig. 8. Power capability chart for cable #a; $d = 120$ km.

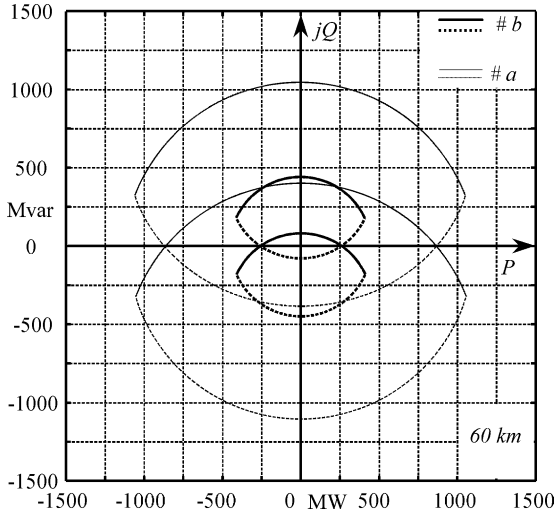


Fig. 9. Power capability chart comparison between cable #b and cable #a; $d = 60$ km.

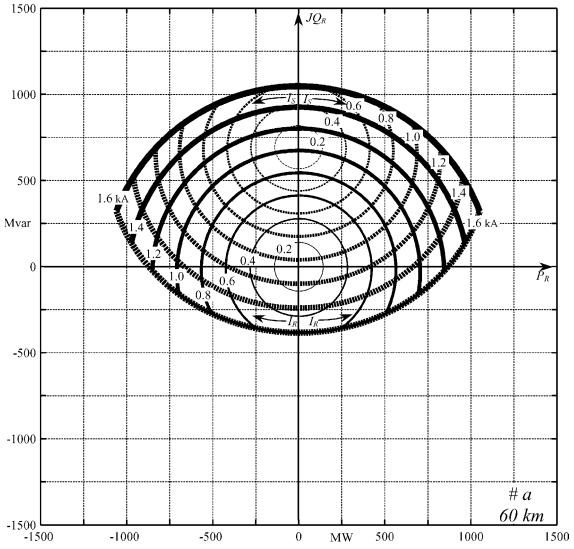


Fig. 10. Enhanced capability chart at receiving-end for cable #a; $d = 60$ km.

dashed line c with parameter $|\underline{I}_S| = 1.6$ kA (exactly it would be 1.62 kA as in Table 3).

Even the only analysis of these few cases ($d = 30$, 60, 90 and 120 km) seems to highlight very well how, in the use of EHV cable, the first important problems, (which increase with the length $d$) are the difficulties to have consistent active power flows with high $\cos\varphi$ (shadowed areas in Fig. 7); only successively (see Table 3), the Ferranti effect and the no-load current take a predominant and decisive role. This could be drastically inverted if "weak networks" are considered (as it could be shown in further researches). The main responsible of these problems is the well-known high capacitive susceptance, which has to be sensibly compensated by means of shunt reactors.

The analyses up to here have been performed for cable #a over different lengths: if cable #b is considered, the features become slightly worse. For instance, the comparison in Fig. 9, performed for $d = 60$ km, shows that cable #b suffers in the maximum transmissible active power a stronger reduction than in the ampacity and a worsening in the corresponding power factor. Table 4 reports the no-load conditions of cable #b and is worth comparing with Table 3 of cable #a.

Furthermore, it could be useful for transmission system operators to enhance the capability chart (see Fig. 10) adding also the curves referring to current values less than cable ampacity so that for each transmissible complex power the margins are immediately evident. For computation of the curves in Fig. 10 a single procedure (less heuristic but more direct)

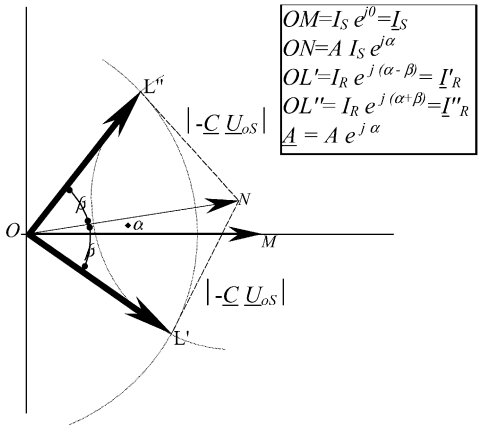


Fig. 10.bis. Triangles for Briggs formula application.

can be adopted alternatively to analysis in Sections 3 and 4: it is based upon Eq. (A10) and Fig. 10.bis. It is sufficient to note that the value of $\beta$ can be derived by means of well-known Briggs formula applied on the two triangles OL′N and OL″N (once set the magnitudes of their sides $|\underline{A}||\underline{I}_S|$, $|\underline{I}_R|$ and $|-\underline{C}\underline{U}_{oS}|$, which have to be geometrically compatible). Eq. (A10) must be obviously computed twice for both $I'_R = I_R\, e^{j(\alpha-\beta)}$ and $\underline{I}_R'' = I_R\, e^{j(\alpha+\beta)}$.

The calculations of $\underline{U}_{oS}$ and $\underline{U}_{oR}$ and the complex power are rather immediate.

Table 4
Current and voltage magnitudes in no-load condition

| Cable #b | | Cable length $d$ (km) | | | | |
|---|---|---|---|---|---|---|
| | | 30 | 60 | 72.5 | 90 | 120 |
| No-load at R; $\|\underline{U}_{oS}\| = 230$ kV | Current magnitude at S (kA) | 0.27 | 0.54 | 0.65 | 0.81 | 1.11 |
| | Phase-to-earth voltage magnitude at R (kV) | 230.6 | 232.3 | 233.4 | 235.3 | 239.6 |

## 7. Effects of shunt compensation

If the hypothesis of uniformly distributed compensation is retained, the abovementioned procedures are still valid: in fact, once the new admittance $\underline{y}$ (function of the compensation degree $\xi_{sh}$) has been computed by means of (A12) and once all the other parameters ($\underline{k}$, $\underline{Z}_0$, and so on) have been updated, all the aforementioned procedures (Sections 3–6) can be suitably used in order to evaluate the compensation effects. This hypothesis, notwithstanding being merely theoretical, presents small differences from real installation techniques [10]. The capability charts of Fig. 11 evidence (with an immediate comparative view) the more or less advantageous effects depending upon $\xi_{sh}$ for cable #a. The comparison between Table 3 and Table 5 shows how small $\xi_{sh}$ can render permissible the no-load regimes up to great lengths. Furthermore, it should be noted that also the length $d = 120$ km can be fully re-qualified if $\xi_{sh} = 0.85$.

As a result of application of an increasingly higher compensation degree $\xi_{sh}$ (from 0.5 to 0.85), the cable line increasingly approaches to a mere series impedance (ohmic–inductive one).

This effect yields higher voltage drop for reactive power flows: in the capability charts, the "upper" grey-solid curves represent regimes with too low voltage profiles (i.e. $|\underline{U}_{oR}| < 215$ kV) whilst the "lower" ones regimes with too

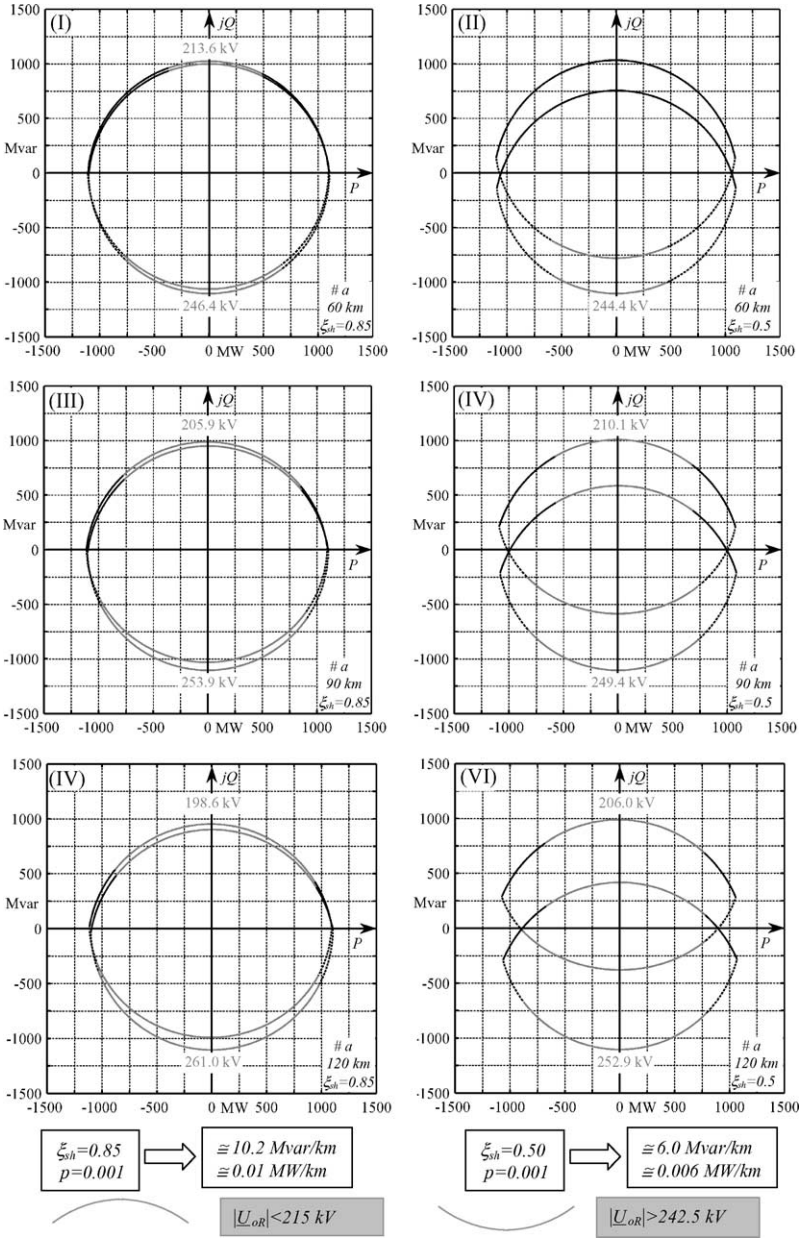


Fig. 11. Power capability charts for cable #a with $d = 60$, 90 and 120 km and $\xi_{sh} = 0.85$; 0.5.

Table 5
Current and voltage magnitudes in no-load condition with two different $\xi_{SH}$

| Cable #a | | Cable length $d$ (km) | | |
|---|---|---|---|---|
| | | 60 | 90 | 120 |
| $\xi_{sh} = 0.50$ | Current magnitude at S (kA) | 0.525 | 0.795 | 1.076 |
| | Phase-to-earth voltage magnitude at R (kV) | 232.8 | 236.4 | 241.6 |
| $\xi_{sh} = 0.85$ | Current magnitude at S (kA) | 0.16 | 0.235 | 0.315 |
| | Phase–to–earth voltage magnitude at R (kV) | 230.8 | 231.9 | 233.4 |

Table 6
Typical data of 400 kV GIL under study

| Gas insulated line | |
|---|---|
| Cross sectional area of phase (Al IACS = 61%) ($mm^2$) | 5341 |
| Cross sectional area of enclosure (Al alloy IACS = 52.57%) ($mm^2$) | 16022 |
| Phase outer diameter (mm) | 180 |
| Phase thickness (mm) | 10 |
| Enclosure inner diameter (mm) | 500 |
| Enclosure thickness (mm) | 10 |

high voltage profiles (i.e $|\underline{U}_{oR}| > 420/\sqrt{3}$); the grey-printed values indicate the minimum and maximum voltages at R, respectively.

## 8. Cables with gas insulation: GILs

The proposed procedure has been suitably applied to another kind of cable with gas mixture insulation namely gas insulated transmission line [11]: Tables 6 and 7 report the typical data and the parameters used in the following analysis.

From Table 7 it is of note the low per unit length capacitance $c$ (54.5 nF/km) and the high ampacity (2400 A).

By using Eq. (A11) the following no-load voltage and current limit lengths arise, respectively:

$$d_U = 308\,\text{km}; \qquad d_I = 542\,\text{km}$$

Table 7
Parameters of 400 kV GIL under study

| Gas insulated line | |
|---|---|
| Installation | Directly buried flat with axial spacing 1.3 m |
| Per unit length resistance of phase at 60 °C, $r_{ph}$ (mΩ/km) | 6.286 |
| Per unit length resistance of enclosure at 50 °C, $r_{en}$ (mΩ/km) | 2.330 |
| Per unit length series inductance, $\ell$ (mH/km) | 0.204 |
| Per unit length shunt leakage, $g$ (nS/km) | Negligible |
| Per unit length shunt capacitance, $c$ (μF/km) | 0.0545 |
| Characteristic impedance, $\underline{Z}_0$ (Ω) | 61.46∠−0.07 rad |
| Propagation factor, $\underline{k}$ ($km^{-1}$) | 0.0001 + j0.001 |
| Surge impedance loading at 400 kV, SIL (MVA) | 2604 |
| Capacitive current related to $U_o = 400\,\text{kV}/\sqrt{3}$, $I_{cap}$ (A/km) | 3.95 |
| Ampacity, $I_c$ (A) | 2400 |

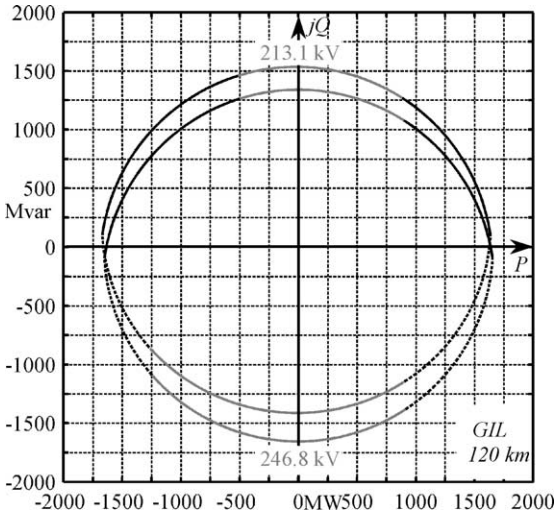


Fig. 12. Power capability chart for GIL; $d = 120$ km.

It is worth noting that the limit $d_U$ is much more restrictive than $d_I$. Also the other criterion, which deals with the power capability, is few limiting: both Fig. 12 ($d = 120$ km) and Fig. 13 ($d = 240$ km) highlight that GILs are suitable for bulk power transmission even if without compensation. This good behaviour fades slightly up to 300 km. The ultimate retained criteria are the voltages and currents along the GIL: the current magnitudes never exceed the ampacity whereas

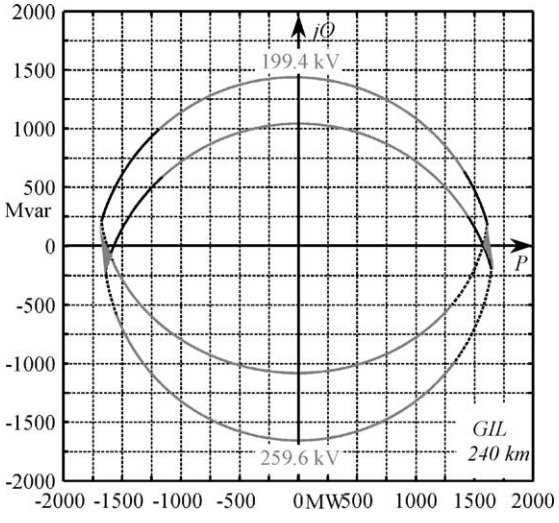


Fig. 13. Power capability chart for GIL; $d = 240$ km.

the regimes exceeding the voltage limit are highlighted in Figs. 12 and 13 by means of grey lines; this confirms the well-known difficulties to transmit high reactive power flows over long distances. The capability chart (along with "grey warnings") computed for higher ampacity (e.g. $I_c = 3000$ A) would show shorter length limits (100–150 km).

## 9. Regimes with $U_{oc} \neq 230$ kV

In the foregoing cases it has been always set $|U_{oS}| = U_c = 230$ kV according to (3). Other capability charts with $U_{oc}<$ or >230 kV could be helpful to transmission system operators in order to optimise the network regimes in daily load variations.

## 10. Conclusion

The paper gives efficient means in order to evaluate the power capability of EHV ac cables. The power capability chart represents an immediate and precise outlook on the possibilities of active and reactive power flows along the link. In each capability chart, the regimes that give rise to receiving-end voltages too high or too low are highlighted. The voltage and current magnitudes in any point along the cable have been also considered. The cable limit lengths can be overcome by means of shunt compensation: the capability charts show the different benefits depending upon the compensation degree. The procedure has been also successfully applied to gas insulated transmission lines showing promising performance in power transmission. The method is based on the classic transmission formulae and has been fully developed in matrix form.

## Acknowledgements

The authors gratefully acknowledge both Ing. Claudio Di Mario (Italian GRTN–Grid Division) for having appreciated the paper aims and Prof. Rudolf Woschizt (Institute of High Voltage Engineering, University of Graz) for having given some technological data on shunt reactors.

## Appendix A

The Eqs. (4) and (5) can be rearranged in matrix form:

$$\begin{bmatrix} \underline{U}_{oS} \\ \underline{I}_S \end{bmatrix} = \underbrace{\begin{bmatrix} \underline{A} & \underline{B} \\ \underline{C} & \underline{A} \end{bmatrix}}_{\underline{\boldsymbol{M}}} \cdot \begin{bmatrix} \underline{U}_{oR} \\ \underline{I}_R \end{bmatrix} \tag{A1}$$

where

$\underline{A} = \cosh(\underline{k}d)$; $\underline{B} = \underline{Z}_0 \cdot \sinh(\underline{k}d)$;

$\underline{C} = [\sinh(\underline{k}d)]/\underline{Z}_0$;

$d$ (km) cable length;

$\underline{k} = \sqrt{\underline{z} \cdot \underline{y}}\,(\mathrm{km}^{-1})$ propagation factor;

$\underline{Z}_0 = \sqrt{\dfrac{\underline{z}}{\underline{y}}}\,(\Omega)$ characteristic impedance;

$$\underline{z} = r + \mathrm{j}\omega\ell\,(\Omega/\mathrm{km}); \qquad \underline{y} = g + \mathrm{j}\omega c\,(\mathrm{S/km}); \tag{A2}$$

$r$ (Ω/km); $\ell$ (H/km); $c$ (F/km); $g = \omega c \tan\delta$ (S/km).

These values can be easily computed or obtained by means of cable manufacturers.

The Eqs. (6) and (7) used in the first analysis can be synthesized by

$$\begin{bmatrix} \underline{U}_{oR} \\ \underline{I}_S \end{bmatrix} = \underbrace{\begin{bmatrix} 1/\underline{A} & -\underline{B}/\underline{A} \\ \underline{C}/\underline{A} & 1/\underline{A} \end{bmatrix}}_{\underline{\boldsymbol{M}}_1} \cdot \begin{bmatrix} \underline{U}_{oS} \\ \underline{I}_R \end{bmatrix}, \tag{A3}$$

whilst Eqs. (8) and (9) of the second analysis by means of

$$\begin{bmatrix} \underline{U}_{oR} \\ \underline{I}_R \end{bmatrix} = \underbrace{\begin{bmatrix} \underline{A} & -\underline{B} \\ -\underline{C} & \underline{A} \end{bmatrix}}_{\underline{\boldsymbol{M}}_2} \cdot \begin{bmatrix} \underline{U}_{oS} \\ \underline{I}_S \end{bmatrix}. \tag{A4}$$

From (A4) it is rather immediate to achieve

$$\begin{bmatrix} \underline{U}_{ox} \\ \underline{I}_x \end{bmatrix} = \underbrace{\begin{bmatrix} \underline{A}_x & -\underline{B}_x \\ -\underline{C}_x & \underline{A}_x \end{bmatrix}}_{\underline{\boldsymbol{M}}_{\boldsymbol{x}}} \cdot \begin{bmatrix} \underline{U}_{oS} \\ \underline{I}_S \end{bmatrix}, \tag{A5}$$

which allows calculating the voltages and currents along the cable (at a distance $x$ from S) having $\underline{A}_x$, $\underline{B}_x$ and $\underline{C}_x$ obvious meaning.

By observing the diagrams of Figs. 3–6 it is sufficient to calculate (similarly to (A5)) simply the mid-line values $U_{oT}$ and $I_T$ by means of

$$\begin{bmatrix} \underline{U}_{oT} \\ \underline{I}_T \end{bmatrix} = \underbrace{\begin{bmatrix} \underline{A}_T & -\underline{B}_T \\ -\underline{C}_T & \underline{A}_T \end{bmatrix}}_{\underline{\boldsymbol{M}}_{\boldsymbol{T}}} \cdot \begin{bmatrix} \underline{U}_{oS} \\ \underline{I}_S \end{bmatrix} \tag{A6}$$

where the subscript T refers to line mid point.

In conclusion, since (A7) can be obtained by (A3)

$$\begin{bmatrix} \underline{U}_{oS} \\ \underline{I}_S \end{bmatrix} = \underbrace{\begin{bmatrix} 1 & 0 \\ \underline{C}/\underline{A} & 1/\underline{A} \end{bmatrix}}_{\underline{\boldsymbol{M}}'} \cdot \begin{bmatrix} \underline{U}_{oS} \\ \underline{I}_R \end{bmatrix}, \tag{A7}$$

the first analysis can be wholly computed with

$$\begin{bmatrix} \underline{U}_{oR} \\ \underline{I}_S \\ \underline{U}_{oT} \\ \underline{I}_T \end{bmatrix} = \begin{bmatrix} \underline{\boldsymbol{M}}_1 \\ \\ \underline{\boldsymbol{M}}_T\underline{\boldsymbol{M}}' \\ \\ \end{bmatrix} \cdot \begin{bmatrix} \underline{U}_{oS} \\ \underline{I}_R \end{bmatrix}. \tag{A8}$$

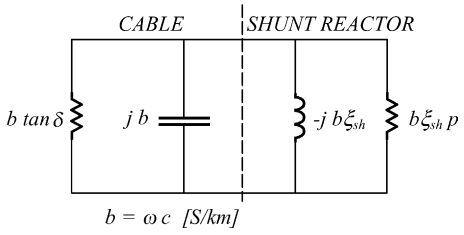


Fig. A1. Shunt branch with compensation reactor per km.

The second analysis can be performed with

$$\begin{bmatrix} \underline{U}_{oR} \\ \underline{I}_{R} \\ \underline{U}_{oT} \\ \underline{I}_{T} \end{bmatrix} = \begin{bmatrix} \underline{\boldsymbol{M}}_2 \\ \\ \underline{\boldsymbol{M}}_T \end{bmatrix} \cdot \begin{bmatrix} \underline{U}_{oS} \\ \underline{I}_{S} \end{bmatrix}. \tag{A9}$$

The sending-end and receiving-end power can be suitably achieved as well.

Furthermore, it is worth remembering the matrix relation

$$\begin{bmatrix} \underline{U}_{oS} \\ \underline{U}_{oR} \end{bmatrix} = \underbrace{\begin{bmatrix} \underline{A}/\underline{C} & -1/\underline{C} \\ 1/\underline{C} & -\underline{A}/\underline{C} \end{bmatrix}}_{\underline{\boldsymbol{Z}}} \cdot \begin{bmatrix} \underline{I}_{S} \\ \underline{I}_{R} \end{bmatrix} \tag{A10}$$

where the impedance matrix $\underline{\boldsymbol{Z}}$ is involved (with the same phasor conventions).

As regards no-load conditions (of an uncompensated lossless line whose characteristic impedance $Z_0$ is purely real and the propagation factor $k = \mathrm{j}k''$ is purely imaginary), once set the voltage level $U_{oS}$ and the ampacity $I_c$, two transmission length limits arise if $U_{oR} = U_m/\sqrt{3}$ and $I_S = I_c$ (angles in rad):

$$d_U = \left(\frac{1}{k''}\right) \cdot a \cos\left(\frac{U_{oS}\sqrt{3}}{U_m}\right);$$

$$d_I = \left(\frac{1}{k''}\right) \cdot a \tan\left(Z_0 \frac{I_c}{U_{oS}}\right) \tag{A11}$$

As regards cables (if considered lossless) this would mean

| | | |
|---|---|---|
| Cable #a | $d_U = 87.68$ km; | $d_I = 89.02$ km; |
| Cable #b | $d_U = 136.4$ km; | $d_I = 72.4$ km. |

If uniformly distributed shunt compensation is considered, the expression of shunt admittance $\underline{y}$ becomes (see Fig. A1)

$$\underline{y} = b \cdot \tan\delta + b \cdot \xi_{sh} \cdot p + \mathrm{j}b \cdot (1 - \xi_{sh}); \tag{A12}$$

where $b\,p\,\xi_{sh} = g_{sh}$ is the per unit length conductance due to the reactor losses. Eq. (A12) coincides with (A2) if $\xi_{sh} = 0$.

## Appendix B. List of symbols

*Abbreviations and symbols*

| | |
|---|---|
| $\underline{X}$ | complex number; |
| EHV | extra high voltage; |
| XLPE | cross-linked polyethylene; |
| GIL | gas insulated transmission line; |
| AC | alternating current; |
| $U_o$ | phase-to-earth voltage; |
| $U$ | phase-to-phase voltage; |
| $U_{oc}$ | chosen phase-to-earth voltage level; |
| $I_c$ | ampacity; |
| $\omega = 2\pi f$ | angular frequency; |
| $\underline{k} = k' + \mathrm{j}k''$ | propagation factor; |
| $d$ | transmission line length; |
| $x$ | distance from sending-end; |
| $\underline{Z}_0$ | characteristic impedance; |
| $I_n$ | natural or characteristic current; |
| $\ell$ | per unit length series inductance; |
| $c$ | per unit length shunt capacitance; |
| $r$ | per unit length series resistance; |
| $g$ | per unit length conductance (due to the dielectric losses); |
| $g_{sh}$ | per unit length conductance (due to the shunt reactor losses); |
| $\xi_{sh}$ | shunt compensation degree (0–1); |
| $p$ | reactor loss factor; |
| $\tan\delta$ | dielectric loss factor. |

*Subscripts*

| | |
|---|---|
| R | receiving-end; |
| S | sending-end; |
| T | line mid point; |
| o | phase-to-earth. |

## References

[1] J. Bernd, A. Surdur Hansen: XLPE-insulated cable rated up to 400 kV for EHV power transmission, ABB Review, vol. 2, 1994, pp. 13–20.
[2] E. Dorison, X. Bourgeat, Y. Maugain, P. Argaut, P.M. Dejean, P. Mirebeau, Optimizing 400 kV underground links with cross-linked polyethylene insulated cables for bulk power transmission, CIGRÉ (1998) 21–105.
[3] J.R. Attwood, M. Dickinson, B. Gregory, R.N. Hampton, R. Svoma, Development of high stress HV and EHV XLPE cable systems, CIGRÉ (1998) 21–108.
[4] R. Benato, E.M. Carlini, C. Di Mario, L. Fellin, A. Paolucci, R. Turri, Gas insulated transmission lines in railway galleries, in: Proceedings of 2003 IEEE Bologna Power Tech Conference, Bologna, 23–26 June, IEEE Trans. Power Deliv. 20 (2) (2005).
[5] R. Arrighi, Operating characteristics of long links of ac high voltage insulated cables, in the name of WG 21.13, in: International Conference on Large High Voltage Electric Systems, Paper 21–13, CIGRÉ (1986) 1–10.
[6] O. Heaviside, Electrical Papers, vol. 2, second ed., Chelsea Publishing Company, New York, 1970.
[7] C.P. Steinmetz, Engineering Mathematics, McGraw-Hill, New York, 1910.
[8] G. Rössler, Die Fernleitung von Wechselströmen, Springer, Berlin, 1905.
[9] J.L. la Cour, Theorie der Wechselströme und Transformatoren, Springer, Berlin, 1902.

[10] P. Halvarsson, et al., A novel approach to long buried ac transmission system, CIGRÉ 21 (2002) 201.
[11] C.G. Henningsen, G. Kaul, H. Koch, A. Schuette, R. Plath, Electrical and mechanical long-time behaviour of gas-insulated transmission lines, CIGRÉ 21–23 (2000), 33-03.

*Roberto Benato* was born in Venezia, Italy, in 1970. He received the Dr. Ing. degree in electrical engineering from the University of Padova in 1995 and Ph.D. in Power Systems Analysis in 1999. In 2002, he was appointed as Assistant Professor in the Power System Group at the Department of Electrical Engineering at Padova University. His main fields of research are multiconductor analysis, EHV-HV transmission lines and advanced matricial techniques for the static and dynamic power system analysis. He is member of CIGRÉ WG B1.08 “Cable systems in multipurpose or shared structures” and secretary of CIGRÉ JWG B3-B1.09 “High Capability Applications of Long Gas-Insulated Lines in Structures”. He is a member of AEIT.

*Antonio Paolucci* was born in Padova, Italy, in 1924. He received the Dr. Ing. degree in electrical engineering from the University of Padova in 1950. He joined the Department of Electrical Engineering of the University of Padova in 1952 where he was Assistant and later Associate Professor. From 1973 to 2000 he has been Full Professor of Power Systems Analysis. His fields of interest also include design of industry electric power plants and large laboratory research power plants. He is a member of AEIT.